Desalination and Water Treatment
www.deswater.com

doi: 10.1080/19443994.2015.1063091

57 (2016) 14109–14131
June

Taylor & Francis
Taylor & Francis Group

Adsorption of Acid Blue 121 dye on fish (*Dicentrarchus labrax*) scales, the extracted from fish scales and commercial hydroxyapatite: equilibrium, kinetic, thermodynamic, and characterization studies

Deniz Uzunoğlu, Ayla Özer*

Department of Chemical Engineering, University of Mersin, 33343 Yenişehir-Mersin, Turkey, email: denizuzunoglu4@gmail.com (D. Uzunoğlu), Tel. +90 324 361 00 01; Fax: +90 324 361 00 32; emails: ayozer@mersin.edu.tr, ayozer4@gmail.com (A. Özer)

Received 14 January 2015; Accepted 9 June 2015

ABSTRACT

In this study, the adsorption of Acid Blue 121 (AB 121) on fish (*Dicentrarchus labrax*) scales (FS), extracted hydroxyapatite from FS (FHAp), low-cost, and environment-friendly adsorbent, and commercial hydroxyapatite (CHAp) was investigated in a batch system as a function of contact time, initial dye concentration, initial pH, adsorbent concentration, and temperature. The Langmuir, Freundlich, Temkin, and Dubinin–Radushkevich isotherm models were applied to the experimental equilibrium data and it was found that the experimental equilibrium data of AB 121 adsorption fitted well to the Langmuir isotherm model. The monolayer coverage capacities of FS and CHAp for AB 121 adsorption were found as 300.7 and 291.5 mg/g, respectively. It was observed that the pseudo-second-order kinetic model could be used for the prediction of studied adsorption processes kinetics. Both film diffusion and intraparticle diffusion contribute to the rate-limiting mechanism. The thermodynamic parameters showed that AB 121 adsorption on FS and CHAp was exothermic in nature. The Fourier transform infrared spectrometer, X-ray diffraction and scanning electron microscopy, energy dispersive X-ray analyzer and Brunauer, Emmet and Teller surface area analyzer were used for adsorbent characterization studies before and after dye treatment. And also, the reusability of FS was determined by desorption studies.

Keywords: Acid Blue 121; Adsorption; Fish scales; Hydroxyapatite; Waste management

1. Introduction

Nowadays, the public has become more sensitive toward the protection of the environment and general awareness has now increased about the potential adverse effects of industrial effluents contaminate with various pollutants, including dyes on the environment [1]. Many industries like textiles, leather, cosmetics, paper, printing, plastics, etc. use many synthetic dyes to color their products. Thus, effluents from these industries contain various kinds of synthetic dye stuffs. Colored wastewaters from these industries, particularly textile industry, cause serious environmental problems. The presence of very small amounts of dyes in water (less than 1 ppm for some dyes) is highly visible and undesirable [2]. There are many structure varieties such as acidic, basic, disperse, azo, diazo, anthroquinone based, and metal complex dyes [3]. In sequence of their importance, acid dyes are mostly used with certain fiber types such as polyamide, wool, silk, modified acrylic, and polypropylene fibers, and so on [4].

*Corresponding author.

The colored wastewater affects aesthetics, water transparency, and gas solubility in water bodies and can be toxic to aquatic flora and fauna, and this causes severe environmental problems worldwide. Furthermore, most dyes and their metabolites are toxic, carcinogenic, and mutagenic, posing a potential hazard to human health. Hence, for protecting both the environment and the human health, and to respect the government law, many researchers try to find an effective and economical way of dye-containing wastewater treatment. However, removal of dyes from the wastewater is not as easy as it seems because dyes generally have complex aromatic molecular structure with synthetic origin, as aforementioned, which make them more stable and difficult to biodegrade. Therefore, the removal of such colored agents from aqueous effluents is of significant environmental, technical, and commercial importance. Different physical, chemical, and biological methods for the removal of dyes from aqueous solutions, such as coagulation and flocculation, electro-flotation, reverse osmosis, irradiation, membrane filtration, ozonation, adsorption, have been investigated [5]. Recent literature reveals that the adsorption has proven to be an effective and attractive process for the removal of the dye-containing effluents among all the dye removal techniques. Activated carbon has been the most versatile adsorbent for the removal of dyes due to its high removal capacity and ease of operation at large scale. However, high cost of activated carbon restricts its application. This case prompts an increased research interest into the low-cost adsorbents to the commonly used activated carbon [6]. A number of researchers have recently used variety of low-cost adsorbents such as spent cotton seed hull, bio-char, sawdust, and industrial and agricultural byproducts for adsorption of different pollutants from wastewater [7–10].

An alternative inexpensive adsorbent able to reduce the cost of an adsorption system has always been searched. A low-cost adsorbent is defined as one which is abundant in nature, or is a byproduct or waste material from another industry [11]. In this study, we attempt to use fish scales (FS), which are discarded as waste material from the fish industry, as an alternative low-cost adsorbent in the adsorption of acidic dye from aqueous solutions. Generally, FS are considered worthless and inapplicable as a waste. However, FS contain numerous valuable organic and inorganic components, mainly collagen and hydroxyapatite. Moreover, extraction of hydroxyapatite (HAp) from natural resources is promising as an alternative choice for obtainment of HAp and reduces cost from usage of CHAp [12]. HAp is a mineral form of calcium apatite with the formula $Ca_5(PO4)_3(OH)$, but is usually written with the formula $Ca_{10}(PO_4)_6(OH)_2$ to suggest that the crystal unit cell comprises two entities. HAp can be used in various applications such as column packing material for chromatography to separate proteins and enzymes, adsorbent material, medical and dental substances because it is an important inorganic material in biology and chemistry due to its availability structure, ion exchange property, adsorption affinity; hence, they have best owed to this material more attention in the recent times [13].

Moreover, the reusability of adsorbent is very important in terms of the process economy and environmental health. As the dye-loaded natural adsorbents cause disposal problem in the environment due to their hazardous nature. Such problem may overcome with desorption. Both making the process more economical and recycling the adsorbent and adsorbate, desorption of dyes and regeneration of adsorbent should be performed [14].

Considering all of these, in this study, the adsorption of Acid Blue 121 (AB 121) onto scales of *Dicentrarchus labrax* (FS), commercial hydroxyapatite (CHAp) and the extracted hydroxyapatite (FHAp) from FS was investigated in a batch system. The desorption studies of dye-loaded FS were also carried out. Before and after the adsorption, the characterization of the studied adsorbents was performed using Fourier transform infrared spectrometer (FT-IR), X-ray diffraction (XRD), scanning electron microscopy (SEM), energy dispersive X-ray analyzer (EDX) and Brunauer, Emmett, and Teller (BET) surface area analyzer.

2. Material and method

2.1. Preparation of FS

Fish (*D. labrax*) scales (FS) were collected from the fisherman's market located in Mersin, Turkey. Mature FS were washed repeatedly with tap water to remove adhering dust and soluble impurities from their surface. FS were allowed to dry in shade for 48 h. FS were then kept in a drying oven at 110°C till the moisture evaporated. The prepared FS were used directly as an adsorbent without grinding.

2.2. Determination of the point of zero charge of adsorbent

The pH where the net surface charge is zero is called the point of zero charge (pH_{PZC}) or isoelectric point. Several techniques have been used for the determination of pH_{PZC} such as solid addition method, mass titration method, fast titration method, potential method, and so on. The solid addition

method was selected in this study because of its reasonableness and easy enforceability.

The points of zero charge of the FS and CHAp were determined by the solid addition method [15]. Initially, 0.1 M KNO_3 solution was prepared and 45 mL of the solution was transferred to 100 mL-conical flasks. Then, the pH values of the solutions were roughly adjusted from 2.0 to 12 by adding 0.1 M HCl and/or 0.1 M NaOH. The total volume of the solution in each flask was made exactly to 50 mL by adding 0.1 M KNO_3 solution. After the initial pH (pH_i) values of the prepared solutions were then accurately noted, 1.0 g of adsorbent was added to each flask, which were securely capped. The suspensions were then manually shaken and allowed to equilibrate for 48 h with intermittent manual shaking. Afterwards, the final pH values (pH_f) of the supernatants were noted. The differences between the initial and final pH values ($pH = pH_i - pH_f$) were plotted vs. the pH_i values. The points of zero charge for the studied adsorbents were determined from the point intersected *x*-axis.

2.3. Extraction of hydroxyapatite from FS

The hydroxyapatite from fish (*D. labrax*) scales was extracted by alkaline heat treatment method [16]. Initially, FS were deproteinized through external washing with 0.1 M HCl and washed several times with distilled water. Then, FS were treated with 5% (w/v) NaOH, heated and stirred magnetically at 70˚C for 3 h. The fine white precipitate was obtained, washed with distilled water and dried at 60˚C in an oven. For the next step of alkaline heat treatment, 50% (w/v) NaOH was added into the treated powder, heated up to 100˚C and stirred magnetically for 1.0 h. The obtained FHAp powders were washed thoroughly with distilled water until the washing solution became neutral and then dried at 60˚C in an oven.

2.4. Characterization of adsorbents

Perkin Elmer Fourier transform infrared spectrometer (FT-IR) was used for the determination of functional groups in the adsorbent before and after adsorption. Crystal structure of the adsorbent was assessed by XRD analysis, using nickel-filtered Cu Kα radiation in a Philips XPert MPD apparatus operated at 40 kV and 30 mA, in the 2θ range of 10˚–80˚. The morphology of the adsorbent was analyzed by Zeiss/Supra 55 SEM analysis. An energy dispersive X-ray analyzer (EDX) was also used to provide elemental identification and quantitative compositional information of the adsorbent. The surface area of the adsorbent was determined by N_2 adsorption at 76.256 K using Micromeritics ASAP 2020V 3.00 G Brunauer, Emmett, and Teller (BET) surface area analyzer.

2.5. Preparation of dye solutions

Acid Blue 121 (AB 121) supplied by Dye Star with commercial name Telon Blue AGLF, (Color Index (CI): 50310; molecular weight (MW): 735.85; molecular formula (MF): $C_{37}H_{38}N_5NaO_6S_2$; λ_{max}: 610 nm) was of commercial quality and was used without further purification. Dye stock solution (1,000 mg/L) was prepared by dissolving exact quantity of AB 121 in distilled water. Necessary dilutions were made to prepare solutions in the range of initial dye concentrations 25–500 mg/L. The initial pH of each solution was adjusted with 0.1 M HCl and 0.1 M NaOH solutions before mixing with the adsorbents.

2.6. Batch adsorption studies

0.1 g of the adsorbent (FS, CHAp, and FHAp), except for adsorbent concentration experiments, was mixed with 100 mL of the desired initial dye concentration and initial pH in Erlenmeyer flasks. The flasks were agitated on a shaker at constant temperature for 120 min to reach adsorption equilibrium. Samples (3 mL) of adsorption medium were taken before mixing the adsorbent and dye-bearing solution, then at predetermined time intervals (in the range of 0.5–120 min) for the residual dye concentration in the solution. Samples were centrifuged at 3,500 rev/min for 5.0 min and the unadsorbed AB 121 dye concentration in supernatant was analyzed at 610 nm wavelenght with Chebios UV–vis spectrophotometer. Experiments were repeated for different initial pH, initial dye concentration, temperature and adsorbent concentration values.

The adsorbed amount at equilibrium, q_e (mg/g), and the percentage of adsorption (%) were computed as follows:

$$q_e = (C_o - C_e)/X_o \quad (1)$$

$$\text{Percent adsorption } (\%) = ((C_o - C_e) \ / \ C_o) \times 100) \quad (2)$$

where C_o and C_e are the initial and equilibrium dye concentration (mg/L), respectively, and X_o is the adsorbent concentration in solution (g/L).

2.7. Desorption studies from FS

After the adsorption reaches to the equilibrium, the adsorption solution was centrifuged at 3,500 rev/min for 5.0 min and the residual AB 121 concentration in supernatant was analyzed at 610 nm wavelength with spectrophotometer. The dye-loaded FS were dried at 60°C in an oven for 24 h. The pH values of solutions were adjusted from 2.0 to 12 with 0.1 M HCl and/or 0.1 M NaOH solutions. Then 0.1 g of the dye-loaded FS were added into 100 mL of prepared solutions. The flasks were agitated on a shaker at 30°C temperature for 120 min. At the end of desorption time, desorption solutions were centrifuged and the dye concentration in desorption solution was determined by spectrophotometer at 610 nm wavelength. These adsorption/desorption processes were repeated for 8.0 times, to further determine the desorption capability of FS [17].

3. Results and discussion

3.1. Characterization of adsorbents

3.1.1. FT-IR analysis

The FT-IR analysis was performed to identify the possible interactions between the functional groups of adsorbents and dye anions. The FT-IR spectrums of FS, CHAp, and FHAp before dye treatment were shown in Fig. 1, and the characteristic absorption peaks were explained in details in Table 1. FT-IR studies were carried out in the range of 400–4,000 cm^{-1} to have knowledge about chemical structure of the studied adsorbents.

Table 1
FTIR analysis results and comparison of FS, CHAp, and FHAp before adsorption

Peak assignments	FS	CHAp	FHAp
C=O	1,646.21	–	–
N–H	1,541.75	–	–
C–H	1,242.03	–	–
Carbonate $_3$	*1,650–1,300*	*1,650–1,300*	*1,650–1,300*
(m)	1,452.80	–	1,466.20
(m)	1,420.19	–	1,420.08
Phosphate $_3$	*1,193–976*	*1,193–976*	*1,193–976*
(vs)	–	1,091.28	–
(vs)	1,043.60	1,031.44	1,034.92
Phosphate $_1$ (m)	–	963.17	962.6
Carbonate $_2$ (ms)	–	–	873.61
Phosphate $_4$	*700–520*	*700–520*	*700–520*
(m)	675.07	631.17	674.84
(vs)	604.93	601.92	603.89
(vs)	561.84	563.65	566.11

Basically, FS are composed of organic and inorganic compounds. Whether the amounts of these compounds vary by the types of FS, they contain approximately 41–84% organic-based protein, collagen, and the remainder is inorganic-based part, hydroxyapatite. Fig. 1(a), the FTIR spectrum of FS, showed characteristic peaks corresponding to the organic components of the FS, namely amide I, II, and III bands of collagen at the absorption peaks at 1,646,

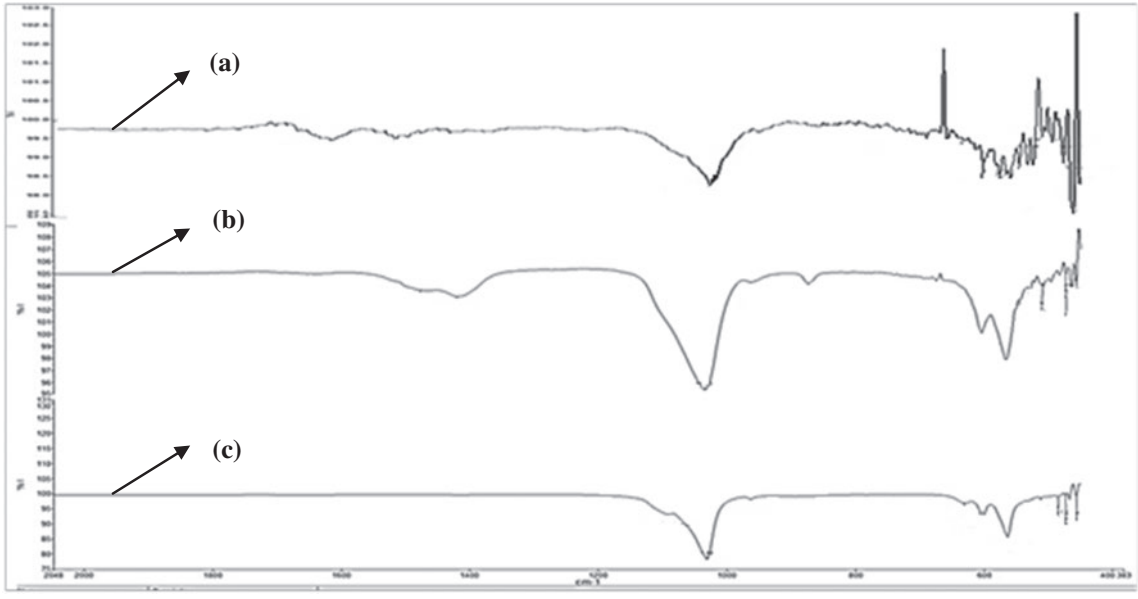

Fig. 1. FTIR spectra of (a) FS, (b) FHAp, and (c) CHAp.

1,541, and 1,242 cm^{-1}, respectively. The amide I peak is associated with the C=O stretching vibrations, the amide II peak is due to the N–H bending vibration and the C–N stretching vibrations, the amide III peak is related to C–N stretching. The inorganic content of FS mainly comes from the hydroxyapatite, so the hydroxyapatite peaks correspond to phosphate and carbonate groups [18]. According to Fig. 1(b) and (c), the perceptible peak at 963 and 962 cm^{-1} was derived from the P–O stretching of PO_4^{3-} group for CHAp and FHAp, respectively. The three sharp peaks between 700 and 520 cm^{-1} corresponded to the triple bending vibrations of phosphate in FS, CHAp, and FHAp. The distinguishable peaks at 1,043, 1,031, and 1,034 cm^{-1} represented the phosphate groups in FS, CHAp, and FHAp, respectively. The bands at 1,466, 1,420, and 873 cm^{-1} for FHAp; 1,452 and 1,420 cm^{-1} for FS were derived from carbonate groups [13,19].

According to Fig. 1 and Table 1; the main functional groups present on surface of FS were collagen and hydroxyapatite (phosphate and carbonate groups). On the other hand, both CHAp and FHAp exhibit the same characteristic peaks, which is confirming successful extraction operation. Nevertheless, the FTIR analysis detected strong peaks at the wavenumbers of the B-type hydroxyapatite, carbonated hydroxyapatite, (873, 1,420 and 1,466 cm^{-1}) while the typical peaks of the A-type hydroxyapatite (880, 1,450, and 1,540 cm^{-1}) were not evident [20]. This case resulted from carbonate groups found in the structure of FS.

The FT-IR spectrums of FS, CHAp, and FHAp after dye treatment were shown in Fig. 2. Comparison of FTIR spectra of dye-loaded adsorbent with FTIR spectra of pure adsorbent did not display significant changes. According to Fig. 2, any bond breaking or formation was not observed after adsorption, but just it was seen that the characteristic FT-IR peaks of FS, CHAp and FHAp were shifted to a little right. This case was evidence that the adsorption of AB 121 onto FS, CHAp, and FHAp were physical processes. Also, the responsible groups for AB 121 adsorption onto FS were not only collagen structure but also hydroxyapatite (phosphate and carbonate groups) while the responsible groups for AB 121 adsorption onto CHAp were only phosphate groups and the responsible groups for AB 121 adsorption onto FHAp were phosphate and carbonate groups [21].

3.1.2. XRD analysis

The XRD patterns of CHAp and FHAp were shown in Fig. 3 in order to determine the crystallinities and phases of the adsorbents before adsorption. All data were picked up over the 2θ range, from 10° to 90°, but the characteristic peaks of the adsorbents were obtained between 20° and 60°. The characteristic peak of the highest intensity for CHAp and FHAp was obtained at a 2θ value of 25.98 corresponding to 2 1 1 plane in all the cases. The presence of broad diffraction peaks suggests that the crystals are small or structurally disordered or both; but no broad diffraction peak was obtained as can be seen from Fig. 3. Meanwhile, the XRD pattern of FHAp was very similar to CHAp, and also both of them fitted well with standard pattern, proving that the main structural features of CHAp could be obtained by extraction from FS. Also, any other phases such as monetite or brushite were not established, suggesting the adsorbents were in pure phases. The shape of the diffraction peaks also indicated that the CHAp and FHAp were well crystallized [22].

The comparisons of XRD patterns of CHAp and FHAp before and after adsorption were shown in Fig. 4 in order to determine the crystallinities and phases of the adsorbents. According to Fig. 4, there were not much significant differences before and after adsorption from XRD patterns of CHAp and FHAp, but AB 121 dye-loaded CHAp and FHAp samples presented higher intensity of diffraction peaks. This suggested that AB 121 anions diffused into the pores and adsorbed mostly by physisorption without altering the structure of the adsorbent [23]. It was another proof that the adsorption of AB 121 onto CHAp and FHAp was physical process, as designated by Dubinin–Radushkevich isotherm model and FT-IR analysis.

3.1.3. SEM and EDX analysis

Information about elemental identifications and quantitative compositions of the adsorbents were obtained by EDX. The results of elemental analysis were given in Table 2. According to Table 2, FS contain all elements of CHAp (C, Ca, O, P) as well as 0.54% mole ratio of N. This case results from amine groups (N–H, amide II peak) in FS as shown in FTIR spectrum. Also, FHAp and CHAp have same elements indicating the content of hydroxyapatite in FS. On the other hand, although the compositions of CHAp and FHAp were expected to be similar with each other, the results were not as expected due to heterogeneous structures of adsorbents. Accordingly, it was determined with the elemental analyses performed at various parts of the surfaces that the same elements but different percentages of the elements were found in different parts of the surfaces.

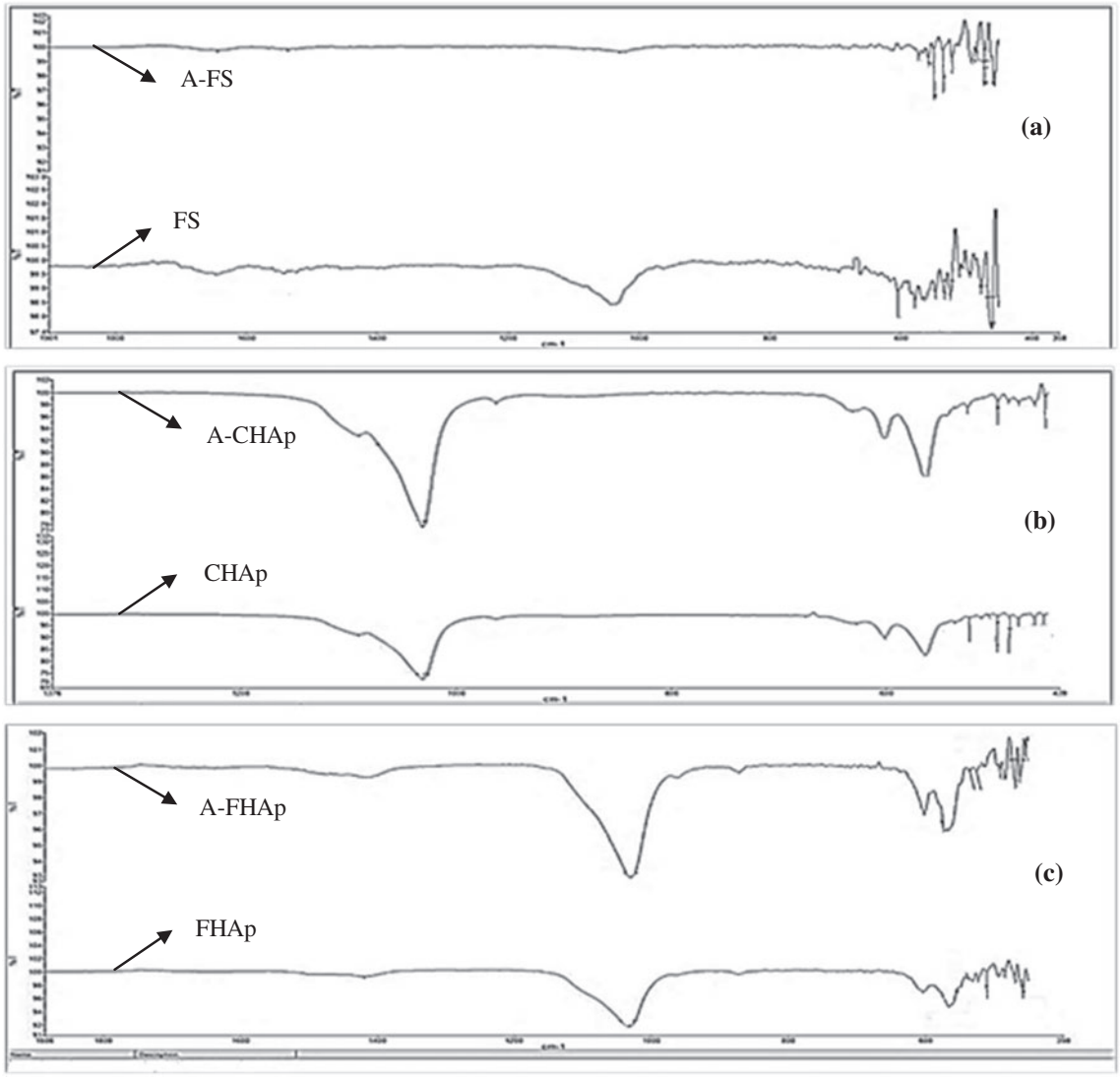

Fig. 2. FTIR spectra before and after (A) adsorption (a) FS, (b) CHAp, and (c) FHAp.

SEM analyses were carried out to investigate the morphologies of the adsorbents before and after AB 121 adsorption. SEM images of FS, CHAp, and FHAp before and after adsorption were shown in Fig. 5. As seen from Fig. 5, any differences between before and after adsorption were not observed. It demonstrated that AB 121 anions were bound to active sites of the adsorbents physically, and any chemical bond formation or breaking did not occur during the adsorption process. This case verified the results of FTIR analyses.

3.1.4. BET analysis

The specific surface areas (S_{BET}), average pore volumes (V_{pore}), average pore widths (D_{pore}), and average particle widths ($D_{particle}$) of FS, CHAp, and FHAp were obtained using the Brunauer, Emmett, and Teller (BET) method and were given in Table 3. Also the average pore diameter was calculated from $D_{particle} = 6/(\rho\ S_{BET})$, where ρ is the particle density (3.16 g/m^3 for CHAp, 3.03 g/m^3 for FHAp). According to Table 3, the average pore width of FHAp is smaller than CHAp, so it has larger specific surface area resulting in high adsorption capacity than CHAp. In addition, International Union of Pure and Applied Chemistry (IUPAC) classifies porous materials into three categories—micropores of less than 2.0 nm in diameter, mesopores between 2.0 and 50 nm, and macropores of greater than 50 nm. In this study, the surface areas originating from macropores (>50 nm)

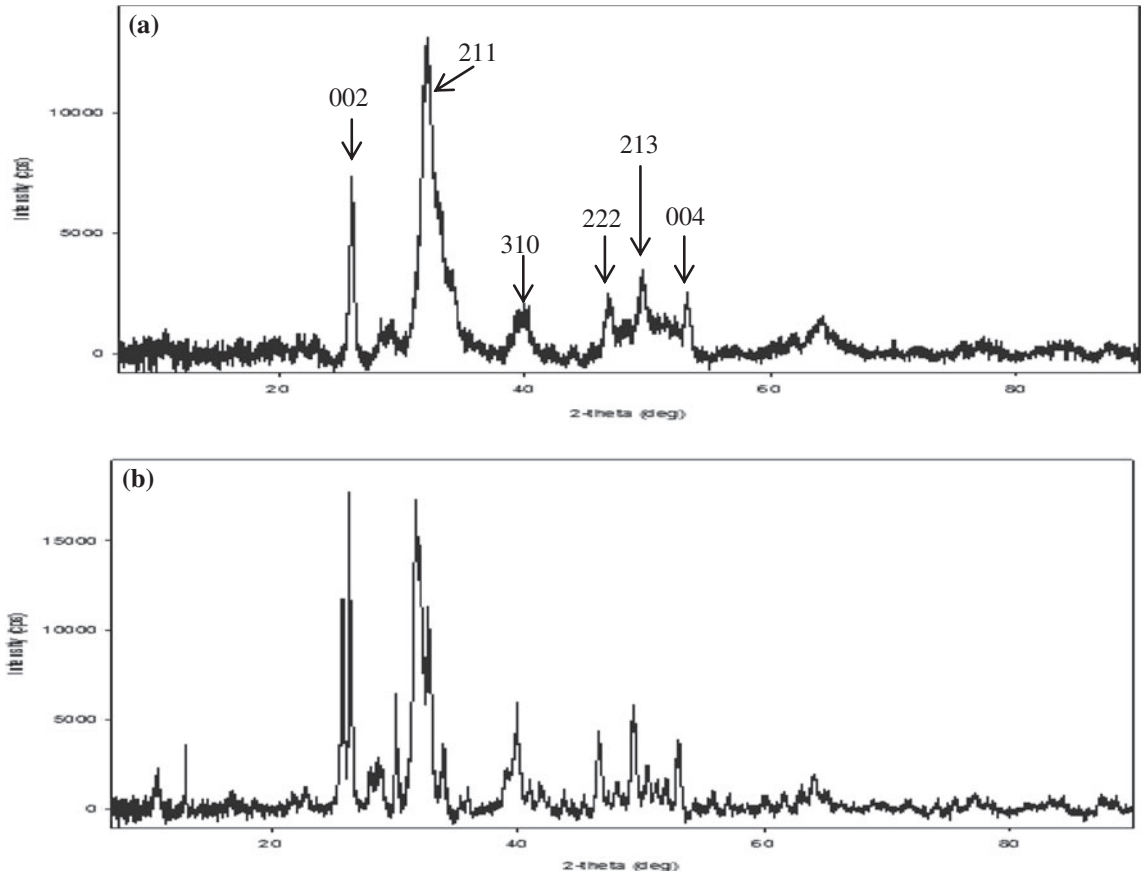

Fig. 3. XRD patterns (a) CHAp and (b) FHAp.

and mesopores (2.0–50 nm) which were estimated by the BJH adsorption pore distribution method. According to pore distribution report, the mesopores composed 38.09, 62.72, and 69.35% of the total volumes of FS, CHAp, and FHAp, respectively. Accordingly, it is clear that a low-cost adsorbent with improved properties (FHAp) was obtained by hydroxyapatite extraction from FS. On the other hand, in descending order of the adsorption capacities are FS, FHAp, and CHAp while this sequence is FHAp > CHAp > FS for specific surface areas. This case could be explained with binding mechanism of dye anions to active sites on the adsorbent surface. Also, the literature review about specific surface areas of the various adsorbents has been done and the specific surface areas of several adsorbents were summarized in Table 4. According to Table 4, the hydroxyapatite extracted from FS in this study has wide surface area than the other adsorbents except for activated carbons. Generally, activated carbons have wide specific surface areas, but their expensive obtainment and difficult regeneration limit their usage as adsorbent. Consequently, the hydroxyapatite extracted from FS is an effective adsorbent, which has low-cost and high specific surface area, for the dye adsorption.

3.2. Optimization studies

Analysis of adsorption data is important for developing equilibrium, kinetic, and thermodynamic parameters that can be used for design purposes. The adsorption of AB 121 onto FS and CHAp was investigated as a function of contact time, initial pH, temperature, initial dye concentration, and adsorbent concentration.

3.2.1. The Effect of initial pH

The pH is one of the most important parameters affecting the adsorption process. The effects of initial pH on adsorption capacities of FS and CHAp were studied in the range of 2.0–5.0 at 100 ± 10 mg/L initial AB 121 concentration, 1.0 g/L adsorbent concentration and 25˚C temperature for 120 min contact time. Fig. 6 presents the effect of initial pH on adsorption of AB

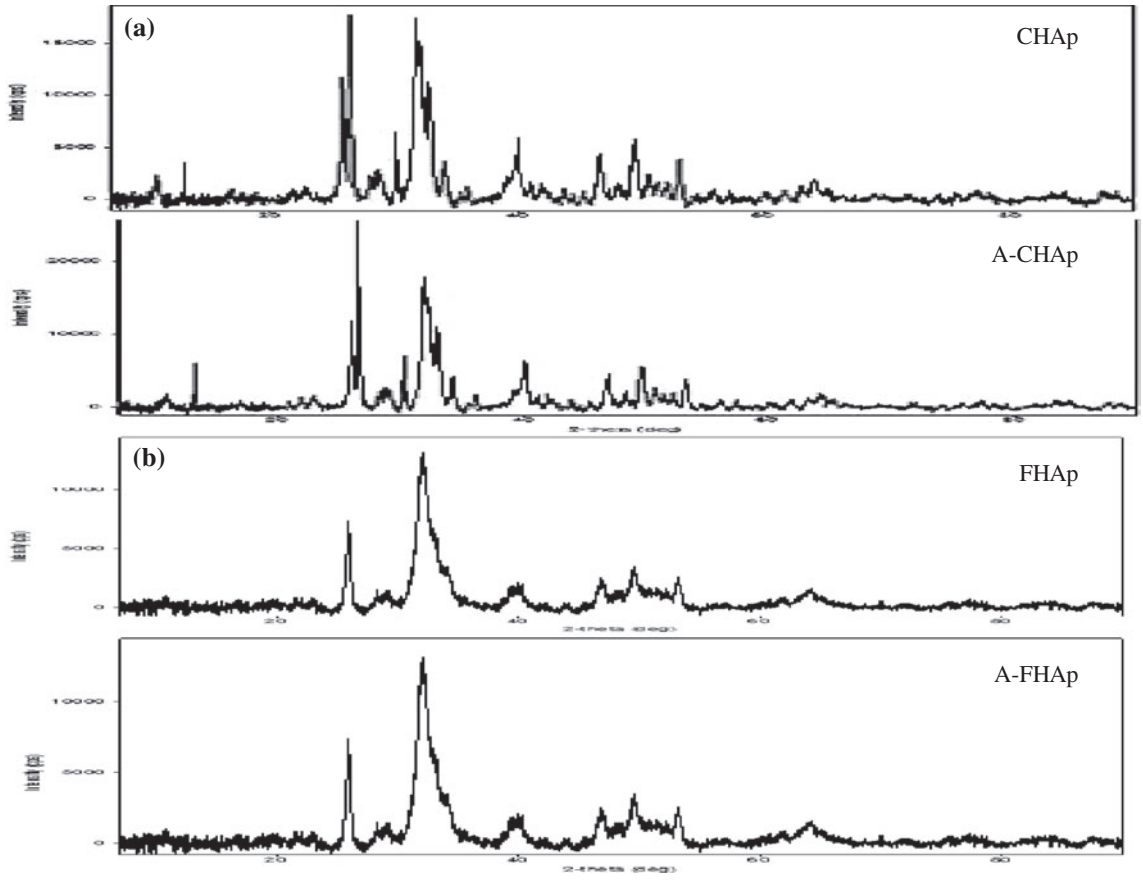

Fig. 4. XRD patterns before and after (A) adsorption (a) CHAp and (b) FHAp.

Table 2
EDX elemental analysis results of FS, CHAp, and FHAp

	Mole (%)		
Element	FS	CHAp	FHAp
Ca	9.6	40.3	25.5
C	40.1	2.07	8.88
O	24.0	27.2	35.0
P	8.47	16.9	7.61
N	0.54	0.35	3.81

121 onto FS and CHAp. As can be seen from Fig. 6, the adsorption capacities of FS and CHAp decreased from 103.2 to 85.6 mg/g and 104.8 to 96 mg/g with increasing initial pH from 2.0 to 5.0, respectively. Also, it was observed that the adsorption percentages decreased from 98 to 77% for FS and from 95 to 87% for CHAp with increasing initial pH from 2.0 to 5.0. The decrease in adsorption with increasing initial pH can be explained on the basis of the pH_{PZC}, which is the point at which the net charge of the adsorbent is zero.

The pH_{PZC} values for FS and CHAp were found as 7.25 and 5.72, respectively. At initial pH < 7.25 for FS and initial pH < 5.72 for CHAp, the surface active sites of the adsorbent may acquire a positive charge leading to increase in anionic dye uptake due to the electrostatic force of attraction. At initial pH 2.0, there is a significantly high electrostatic attraction between the positively charged surface of the adsorbent and dye anions. Therefore, the optimum initial pH was determined as 2.0 for the adsorption of AB 121 onto FS and CHAp. At the pH values > pH_{PZC}, the number of negatively charged sites increases and that of positively charged sites decreases. A negatively charged surface site on adsorbent does not favor the adsorption of dye anions due to the electrostatic repulsion [31].

3.2.2. Effect of initial dye concentration

The effects of initial dye concentration on the AB 121 adsorption by FS and CHAp were investigated in the range of 25–500 mg/L initial AB 121 concentrations at 1.0 g/L adsorbent concentration and 25°C

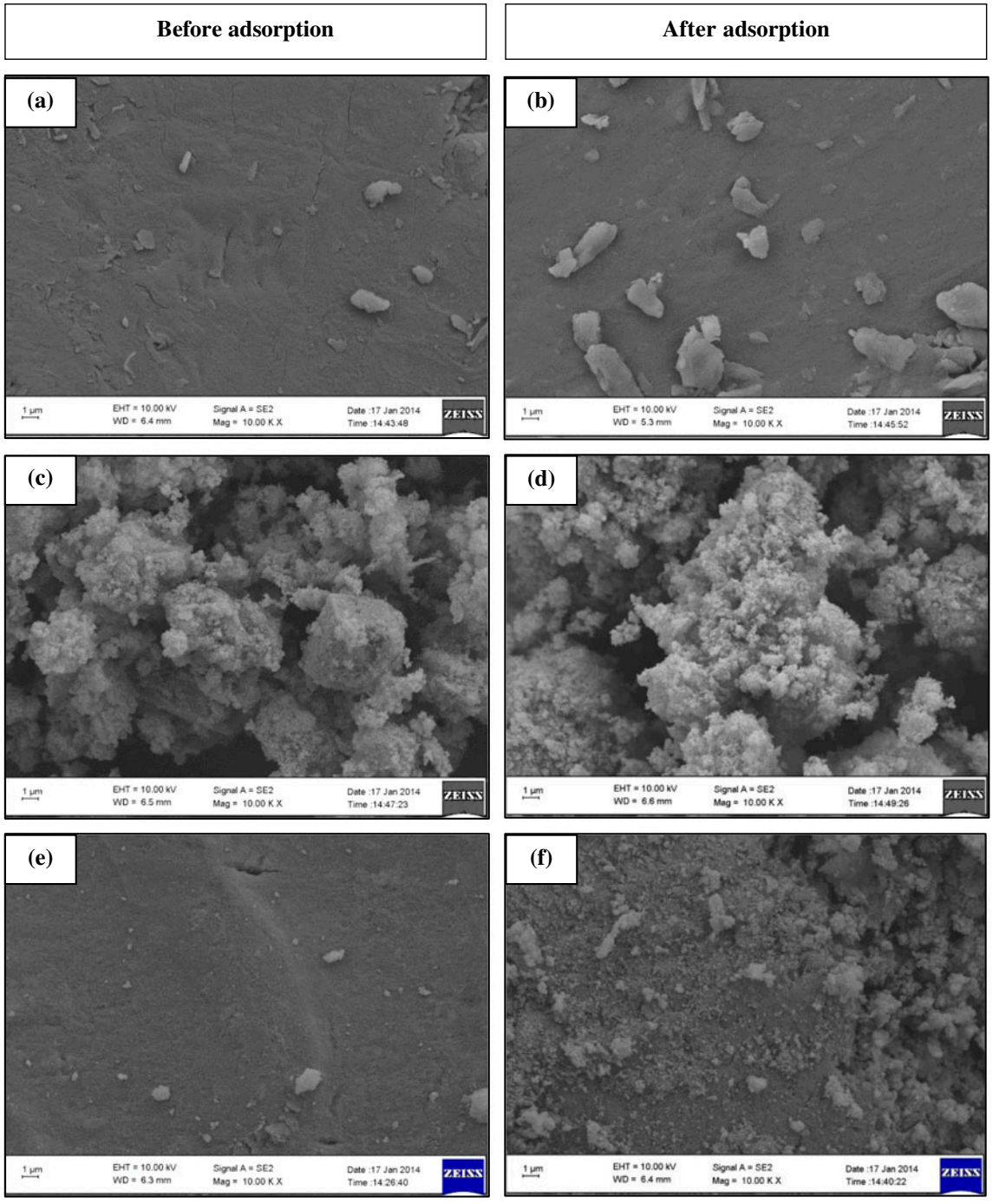

Fig. 5. SEM images of FS (a and b), CHAp (c and d) and FHAp (e and f) before and after adsorption.

temperature for 120 min contact time. The plot of the equilibrium uptake values (mg AB121/g adsorbent) of AB 121 on FS and CHAp vs. the initial dye concentration was presented in Fig. 7. As seen from Fig. 7, the equilibrium uptakes for the studied adsorbents increased with increasing the initial AB 121 concentrations up to 300 mg/L and then did not change with further increase of initial AB 121 concentration. While the initial AB 121 concentration was increased from 25 to 500 mg/L, the uptake amounts increased from 21.6 to 298.4 mg/g for FS, from 20.8 to 277.6 mg/g for CHAp. This is a result of the

Table 3
BET analysis results of FS, CHAp, and FHAp

Parameter	FS	CHAp	FHAp
S_{BET} (m^2/g)	0.83	51.3	94.9
V_{pore} (cm^3/g)	0.0044	0.25	0.28
V_{meso} (cm^3/g)	0.0017	0.15	0.19
V_{macro} (cm^3/g)	0.0027	0.092	0.084
D_{pore} (nm)	16.4	17.0	10.7
$D_{particle}$ (nm)	–	37.0	20.0

increase in the driving force, the concentration gradient, as the initial dye concentration increase. However, the adsorption yields of AB 121 on FS and CHAp decreased from 93.1 to 58.4% and from 92.9 to 57.8%, respectively, as the initial dye concentration was increased from 25 to 500 mg/L. At lower concentrations, all AB 121 dye anions presenting in solution could interact with the binding sites on adsorbent surface and thus the adsorption yields were higher than those at higher initial AB 121 concentrations. At higher concentrations, lower adsorption yield was due

Table 4
The comparison of BET surface areas

Adsorbent	S_{BET} (m^2/g)	Refs.
Sintered UltraCap hydroxyapatite	0.26	[24]
Yttrium-doped nanocrystalline hydroxyapatite	0.29	
Fish (*Dicentrarchus labrax*) scales	0.83	This study
Sintered hydroxyapatite	1.15	[25]
Non-sintered hydroxyapatite	13.3	
Rod-like synthesized hydroxyapatite	29.0	[26]
Spherical synthesized hydroxyapatite	39.0	
Ruthenium/hydroxyapatite catalysts	48.0	[27]
Commercial hydroxyapatite	51.4	This study
Gold/hydroxyapatite catalysts	54.0	[27]
Commercial hydroxyapatite	56.0	
Hydroxyapatite synthesized by wet chemical methods	60.8	[24]
Nanocrystal hydroxyapatite	62.2	[28]
Hydroxyapatite synthesized as mechanochemical	76.1	
Hydroxyapatite extracted from fish (*Dicentrarchus labrax*) scales	94.9	This study
Activated carbon prepared from waste rubber tire	562.0	[29]
Commercial activated carbon	1,168.0	
Activated carbon prepared from mangosteen peel	1,099.0	[30]

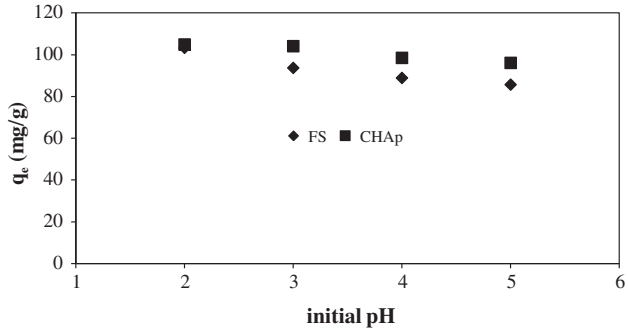

Fig. 6. Effect of initial pH (initial dye concentration: 100 ± 10 mg/L; temperature: 25°C; adsorbent concentration: 1.0 g/L; contact time: 120 min).

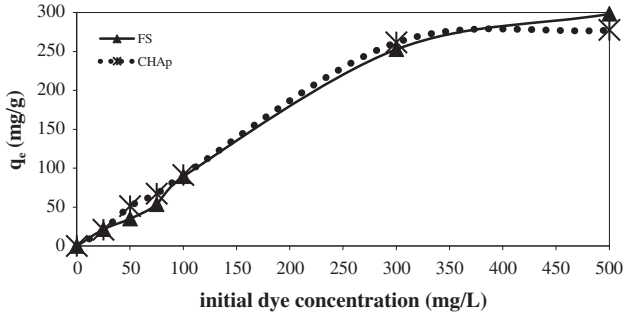

Fig. 7. Effect of initial dye concentration (initial pH 2.0; temperature: 25°C; adsorbent concentration: 1.0 g/L; contact time: 120 min).

to the saturation of adsorption sites. As a result, the purification yield can be increased by diluting the wastewaters containing high dye concentrations [32].

3.2.3. Effect of temperature

The effect of temperature on the AB 121 adsorption by FS and CHAp was investigated in the range of 20–40˚C at 100 ± 10 mg/L initial AB 121 concentration, 1.0 g/L adsorbent concentration and initial pH 2.0 for 120 min contact time and the results were given in Fig. 8. As seen from Fig. 8, the adsorption capacities of the studied adsorbents for AB 121 did not present any remarkable changes in the range of 20–30˚C temperatures, but decreased with further increasing temperature. The adsorption percentages of FS and CHAp for AB 121 dye decreased from 98.4 to 93.7% and 98.4 to 93.6%, respectively, with increasing temperature from 25 to 40˚C. The further increase of temperature may alter the surface activities of FS and CHAp resulting in decrease in adsorption capacities between 30 and 40˚C which means that adsorption processes of AB 121 by FS and CHAp are exothermic in nature. Temperature could influence desorption steps and the reversibility of adsorption equilibrium. This may be due to a tendency of dye molecule transport from the solid phase of adsorbent to the liquid phase of the dye wastewater with increasing temperature [33].

3.2.4. Effect of adsorbent concentration

The adsorbent concentration in aqueous solution plays a substantial role in the adsorption nature. The effect of adsorbent concentration on adsorption of AB 121 by FS and CHAp was investigated in the range of 0.5–3.0 g/L adsorbent concentration at 30˚C, 100 ± 10 mg/L initial AB 121 concentration and initial pH 2.0. The variation of uptake values (mg/g) and the adsorbed AB 121 concentrations (mg/L) with adsorbent concentration were given in Fig. 9. The adsorbed AB 121 amounts per unit mass of adsorbent decreased from 134.4 to 35.2 mg/g for FS, 121.6 to 34.4 mg/g for CHAp with the increase in adsorbent concentration from 0.5 to 3.0 g/L. There are many factors which can contribute to this adsorbent concentration effect. The first and most important factor is that adsorption sites remain unsaturated during the adsorption reaction. This is due to the fact that as the concentration of adsorbent is increased, there is less commensurate increase in adsorption resulting from the lower adsorptive capacity utilization of the adsorbent. The second cause may be the aggregation/agglomeration of sorbent particles at higher concentrations, which would lead to a decrease in the surface area and an increase in the diffusional path length. The particle interaction at higher adsorbent concentration may also help to desorb some of the loosely bound dye anions from the sorbent surface [34]. As can be seen from Fig. 9, it is readily understood that the number of available adsorption sites increased with an increase in adsorbent concentration, therefore, resulted in an increase in adsorbed dye concentration. In this study, further increment in adsorbent concentration from 3.0 g/L did not cause significant improvement in adsorption. This is due to the binding of almost all dye anions to the studied adsorbent and the establishment of equilibrium between dye anions bound to the adsorbent and those remaining unadsorbed in solution.

The adsorption in a batch stirred reactor can be considered as single stage equilibrium. The removal of a given amount of solute can be accomplished with greater economy of adsorbent if the solution is treated with separate small batches of adsorbent rather than in single batch, with filtration between each stage.

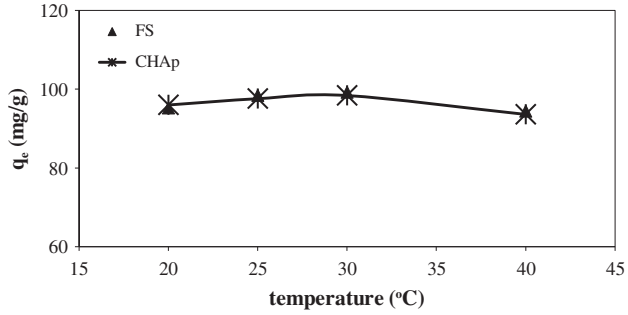

Fig. 8. Effect of temperature (initial pH 2.0; initial dye concentration: 100 ± 10 mg/L; adsorbent concentration: 1.0 g/L; contact time: 120 min).

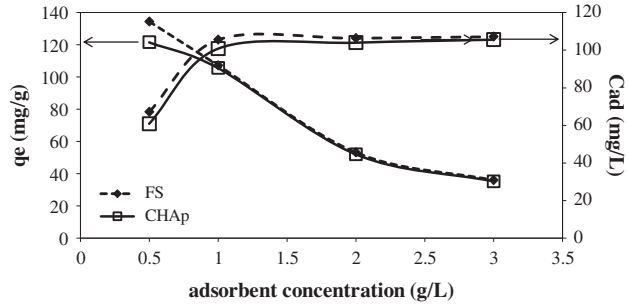

Fig. 9. Effect of adsorbent concentration (initial pH 2.0; temperature: 25˚C; initial dye concentration: 100 ± 10 mg/L; contact time: 120 min).

This method of operation, sometimes called split feed treatment depends on two basic constraints, that of equilibrium and that of a mass balance. The same quantity of solution (V_o) is treated at the single stage by a given amount of adsorbent (X_o) to reduce the dye concentration of solution from C_o to C_e (Fig. 10). The mass balance in the first stage is given by:

$$V_oC_o + X_oq_o = V_oC_{e1} + X_oq_{e1} \quad (3)$$

Eq. (3) can be rearranged;

$$-(V_o/X_o) = (q_{e1} - q_o)/(C_{e1} - C_o) \quad (4)$$

In the same way, for the nth stage:

$$-(V_o/X_o) = (q_{en} - q_o)/(C_{en} - C_{e(n-1)}) \quad (5)$$

The amount (q_o) of dye adsorbed per unit mass of adsorbent at the beginning in each reactor is equal to zero. Eqs. (4) and (5) will provide the operating lines passing through (C_o, q_o) and (C_{e1}, q_{e1}) for the first stage and ($C_{e(n-1)}$, $q_{e(n-1)}$) and (C_{en}, q_{en}) for the nth stage, respectively. Each slope is $-V_o/X_o$, i.e. the negative of the ratio of adsorbent quantity to wastewater volume. If the amounts of adsorbent used in each stage are equal the operating lines are parallel [35].

The equilibrium AB 121 concentrations can also be obtained using the experimental equilibrium curve and operating line. The experimental equilibrium curves (C_e, q_e) and operating lines for the adsorption of AB 121 onto FS and CHAp at 30˚C and initial pH 2.0 were given in Fig. 11(a) and (b), respectively. To determine the equilibrium AB 121 concentration, C_{e1} in solution leaving the first stage, the initial dye concentrations, C_o, (C_o = 312 mg/L for FS and 280 mg/L for CHAp) located at the proper point on the x-axis (C_o, q_o = 0); then the operation lines passing through (C_o, q_o) with a slope of $-V_o/X_o$ = 1.0 are drawn. The intersection of coordinates of the operating line and equilibrium curve gives the abscissa (C_e) and ordinate

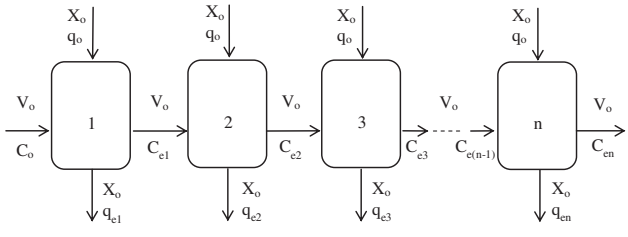

Fig. 10. The adsorption in batch stirred reactors in series.

(q_e) values. As seen from Fig. 11, the operation lines of each stage were parallel because the amount of adsorbent used in each stage was same. The Ministry of Environment and Urbanization of Turkish Republic revised the water pollution control regulation and a water discharge standard related to color parameter has been introduced in 2011. The discharge standard says that the color of wastewater must be below 280 Pt-Co corresponding 35.8 mg/L for AB 121. The desired purification, even values below the standard, could be achieved by two stages in this study as seen from Fig. 11. According to Fig. 11(a) and (b); unadsorbed dye concentrations in solution at the end of the first stage are 36.8 and 36.0 mg/L, at the end of the second stage are 3.0 and 3.2 mg/L for FS and CHAp, respectively. This case is a quite good advantage for a wastewater treatment plant.

3.3. Equilibrium modeling

Equilibrium data, commonly known as adsorption isotherms, describe how adsorbate interacts with adsorbent and so are critical in optimizing the use of adsorbents and provide information on the capacity of the adsorbent [36].

The Langmuir isotherm theory assumes monolayer coverage of adsorbate over a homogenous adsorbent surface. The well-known expression of the Langmuir model is given by Eq. (6) [37];

$$q_e = (Q^o bC_e)/(1 + bC_e) \quad (6)$$

where q_e (mg/g) and C_e (mg/L) are the amount of adsorbed solute per unit mass of adsorbent and unadsorbed solute concentration in solution at equilibrium, respectively. Q^o is the maximum monolayer coverage capacity (mg/g) and b is a constant related to the affinity of the binding sites (L/mg). Q^o represents a practical limiting adsorption capacity when the surface is fully covered with dye molecules and it assists in the comparison of adsorption performance, particularly in cases where the adsorbent did not reach its full saturation in experiments.

The Freundlich expression is an exponential equation and therefore assumes that as the adsorbate concentration increases, the concentration of adsorbate on the adsorbent surface also increases. According to Freundlich model, the amount of adsorbate bound per unit mass of adsorbent at constant temperature is expressed by [38];

$$q_e = K_F C_e^{1/n} \quad (7)$$

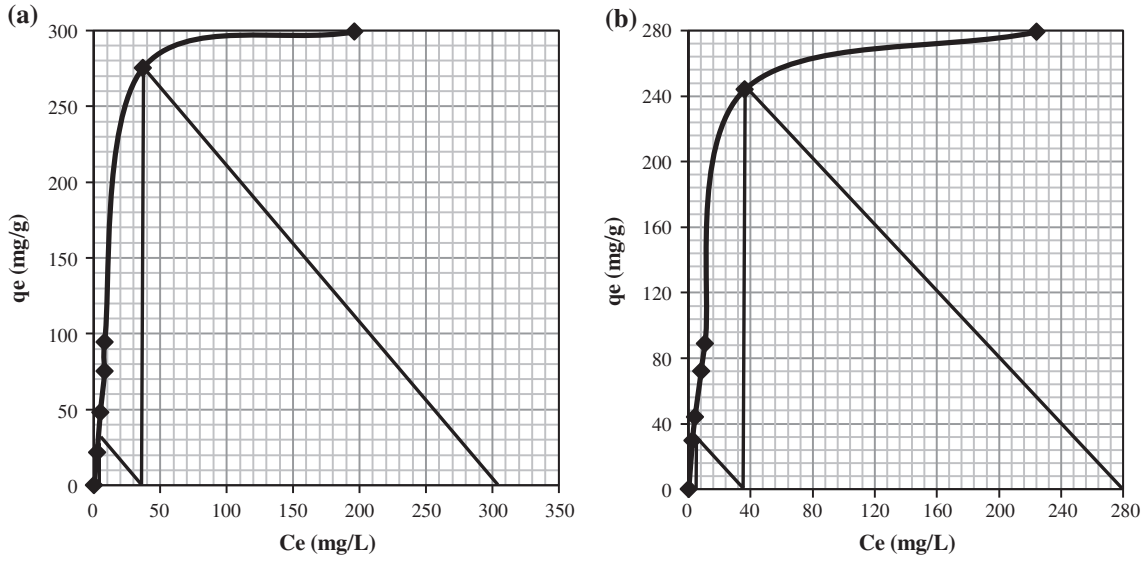

Fig. 11. The equilibrium curves and operation lines with $V_o/X_o = -1.0$ slopes for AB 121 adsorption in the multistage batch reactors (a) FS (initial dye concentration: 312 mg/L; initial pH 2.0; temperature: 25°C; FS concentration: 1.0 g/L; contact time: 120 min) and (b) CHAp (initial dye concentration: 280 mg/L; initial pH 2.0; temperature: 25°C; CHAp concentration: 1.0 g/L; contact time: 120 min).

In this equation, K_F and $1/n$ are the Freundlich constants characteristic on the system, indicating adsorption capacity and intensity, respectively.

Temkin isotherm model explains the effects of some indirect adsorbate/adsorbate interactions on adsorption isotherms and suggests that the heat of adsorption of all the molecules in the layer would decrease linearly with coverage due to these interactions. The equation and its linear form are as follows, respectively [39]:

$$q_e = K_t \ln(AC_e) \tag{8}$$

$$q_e = K_t \ln A + K_t \ln C_e \tag{9}$$

where K_t and A are constants about adsorption heat and maximum binding energy constant, respectively. According to Eq. (9), the Temkin isotherm constants, A and K_t, are determined from slope and intercept of the linear plot of q_e vs. ln C_e.

Dubinin–Radushkevich isotherm model (D–R) is used to paraphrase whether the sorption mechanism is physisorption or chemisorption. It is generally applied to express the adsorption mechanism with a Gaussian energy distribution onto a heterogeneous surface. The non-linear form of the D–R isotherm equation is expressed by [40]:

$$q_e = q_m \cdot e^{-B\varepsilon^2} \tag{10}$$

where q_m is the maximum adsorption capacity (mg/g), B is the activity coefficient related to adsorption mean free energy (mole^2/J^2), and ε is the Polanyi potential [$\varepsilon = RT \ln(1+1/C_e)$]. The adsorption mean free energy is obtained from

$$E = 1/(\sqrt{2B}) \tag{11}$$

The E (kJ/mole) value gives information about adsorption mechanism, and more specially its physical or chemical nature. If it lies between 8 and 16 kJ/mole, the adsorption process is controlled by a chemical mechanism, while for $E < 8$ kJ/mole, the adsorption process proceeds through a physical mechanism [41].

In this study, four famous isotherm models, namely Langmuir, Freundlich, Temkin, and Dubinin–Radushkevich isotherms, were used to correlate experimental equilibrium data for AB 121 adsorption on FS and CHAp at the temperature values of 20, 25, 30, and 40°C, and initial pH 2.0, adsorbent concentration 1.0 g/L, which are the optimum environmental conditions. The corresponding model constants and the regression coefficients were listed in Table 5. The values of regression coefficients (R^2) obtained from the studied models were used as the fitting criteria for comparing these isotherms. As shown from Table 5, the monolayer coverage capacities for AB 121 adsorption were found as 300.7 mg/g for FS and 291.5 mg/g for CHAp from Langmuir isotherm model, at 30°C

which is the optimum temperature. The comparison with the literature of the studied adsorbents was given in Table 6. The results showed that the FS and hydroxyapatite used in this study exhibited higher maximum monolayer adsorption capacity than the others. FS have a higher maximum monolayer coverage capacity than that of CHAp for AB 121 adsorption. This type of behavior can be explained by structural differences of these adsorbents. Also, this case was explained in details in FTIR and BET analysis section. On the other hand, the calculated b values decreased with increasing temperature indicating exothermic nature of the adsorption process.

The mean free adsorption energies from D-R isotherm model (Eq. (11)) for the adsorption processes were calculated to be 227.7 and 442.2 J/mole at 30°C for FS and CHAp, respectively. These results showed that AB 121 adsorption on FS and CHAp proceeds through a physical mechanism due to the free adsorption energies lower than 8.0 kJ/mole. This case verified the results of SEM and FTIR analyses. Vu et al. [52] determined that the free adsorption energy of adsorption of Cu(II) from aqueous solution by anatase mesoporous TiO_2 nanofibers prepared via electrospinning to be 816 ± 376 J/mole, and they concluded that the adsorption process was based on the physical adsorption principles.

The experimental equilibrium data of AB 121 adsorption on FS and CHAp were also evaluated according to Temkin isotherm model equation and the isotherm constants calculated at different temperatures were also presented in Table 5. As can be seen from Table 5, the constant B values, relating to the heat of adsorption, increased with increasing temperature, indicating exothermic adsorption.

The comparison of the experimental and calculated equilibrium data for AB 121 adsorption on FS and CHAp were presented in Fig. 12 along with their error values. An error function is defined to enable the optimization process and to evaluate the fit of the isotherm equation to the experimental data. In this study, the average relative error (ARE) function was examined. ARE function minimizes the fractional error distribution across the entire concentration range [53]:

Table 5
The isotherm model constants (initial pH 2.0; adsorbent concentration: 1.0 g/L; contact time: 120 min)

Adsorbent	Fish scales			Commercial hydroxyapatite		
	Langmuir isotherm					
Temperature (°C)	Q^o	b	R^2	Q^o	b	R^2
20	279.9	0.043	0.998	264.5	0.033	0.996
25	289.1	0.031	0.993	280.1	0.023	0.994
30	300.7	0.018	0.993	291.5	0.013	0.999
40	274.7	0.015	0.995	263.9	0.026	0.998
	Freundlich isotherm					
	$1/n$	K_F	R^2	$1/n$	K_F	R^2
20	0.94	8.9	0.993	0.77	10.8	0.973
25	0.86	9.4	0.989	0.79	8.3	0.960
30	0.65	10.9	0.992	0.66	7.6	0.984
40	0.77	6.1	0.990	0.81	8.1	0.980
	Temkin isotherm					
	A	B	R^2	A	B	R^2
20	0.39	103.3	0.978	0.53	46.8	0.990
25	0.36	105.1	0.986	0.77	47.9	0.980
30	0.24	108.1	0.996	0.59	48.2	0.991
40	0.32	113.7	0.959	0.65	62.9	0.983
	Dubinin–Radushkevich Isotherm					
	q_m	E	R^2	q_m	E	R^2
20	170.2	310.4	0.989	97.9	376.9	0.988
25	172.1	320.8	0.988	98.6	563.4	0.991
30	171.8	227.7	0.999	96.7	442.2	0.989
40	168.9	318.2	0.995	94.3	597.7	0.999

Notes: Q^o (mg/g), b (L/mg), K_F (mg/g)/(L/mg)$^{1/n}$), A (L/g), B (mole^2 J^2), K_t (J/mole), q_m (mg/g), E (kJ/mole).

Table 6
The comparison of the studied adsorbents with adsorbents in the literature

Adsorbent	Adsorbate	Q^o (mg/g)	Ref.
Synthesized poorly crystalline hydroxyapatite	Disperse Blue SBL	434.78	[42]
Fish (*Dicentrarchus labrax*) scales	Acid Blue 121	300.66	This study
Commercial hydroxyapatite	Acid Blue 121	291.46	This study
Fish (*Labeo rohita*) scales	Pb(II)	196.80	[43]
Fish (*Gadus morhua*) scales	Pb(II)	80.00	[44]
Fish (*Oreochromis niloticus*) scales	Cu(II)	58.00	[45]
Hydroxyapatite	Reactive Yellow 84	50.25	[46]
Poly (glutaraldehyde)-stabilized fish (*Micropogonias furnieri*) scales	Cr(VI)	39.00	[47]
Fish (*Labeo rohita*) scales	Malachite Green	38.46	[48]
Chemically modified fish (*Corvina*) scales	Cr(VI)	22.00	[49]
Hydroxyapatite	Phenol	10.33	[50]
Nanocrystalline hydroxyapatite from fish (*Tilapia nilotica*) scales	Se	1.94	[51]
Hydroxyapatite		1.76	
Fish (*Tilapia nilotica*) scales		1.02	

$$\mathrm{ARE} = (100/P)\cdot\sum_{i=1}^{i=P}\left[\left(q_{e,cal}-q_{e,exp}\right)/q_{e,exp}\right] \quad (12)$$

where P indicates the number of measurements. As seen in Fig. 12, the error values (ARE) obtained from the Langmuir isotherm model are lower than Freundlich isotherm model. In addition, the regression coefficients (R^2) obtained from the Langmuir isotherm model are better than those of the other studied isotherm models as seen from Table 5. As a result, the Langmuir isotherm model fitted well to the adsorption data of AB 121 on FS and CHAp.

3.4. Kinetic modeling

Adsorption kinetics models are used to explain the adsorption mechanism and characteristic and rate-controlling step. In this study, the kinetics of the studied adsorption processes were examined using the pseudo-first-order kinetic model (PFOKM), pseudo-second-order kinetic model (PSOKM), intraparticle diffusion model, and Boyd model.

The PFOKM equation was proposed by Lagergren and was the first kinetic equation for the adsorption process [54]. The linear form of the PFOKM equation can be expressed as follows:

$$\log\left(q_e-q_t\right)=\log\left(q_e\right)-(k_1/2.303)t \quad (13)$$

where q_t (mg/g) are the amount of adsorbed solute per unit mass of adsorbent at any time t, k_1 is the pseudo-first-order kinetic rate constant (1/min).

The PFOKM rate constant values (k_1) for AB 121 adsorption on FS and CHAp were determined from the plot of $\log(q_e-q_t)$ vs. t at different initial AB 121 dye concentrations (not shown figure) and were given in Table 7.

The PSOKM equation was proposed by Ho and McKay [54] and it was derived on the basis of the sorption capacity of the solid phase. The linear form of the PSOKM equation can be expressed as follows:

$$\left[t/q_t\right]=\left[1/k_2q_e^2\right]+\left[t/q_e\right] \quad (14)$$

where k_2 is the PSOKM constant (g/(mg min)).

The PSOKM rate constant values (k_2) for AB 121 adsorption on FS and CHAp were determined from the plot of t/q_t vs. t at different initial AB 121 dye concentrations (not shown figure) and were given in Table 7. The comparison of the experimental and calculated q_t values was presented in Table 7 and Fig. 13. As can be seen from Table 7 and Fig. 13, the R^2 values of the PSOKM exceed 0.99 and the q_t values calculated from PSOKM were more consistent with the experimental q_t values than those calculated from the PFOKM. Hence, the PSOKM could be used for the prediction of the kinetics of adsorption of AB 121 on FS and CHAp. Considering the effect of contact time, the uptake amounts increased with increasing the contact time up to 30 min and then remained nearly constant with further increase in contact time for all initial dye concentrations as seen from Fig. 13.

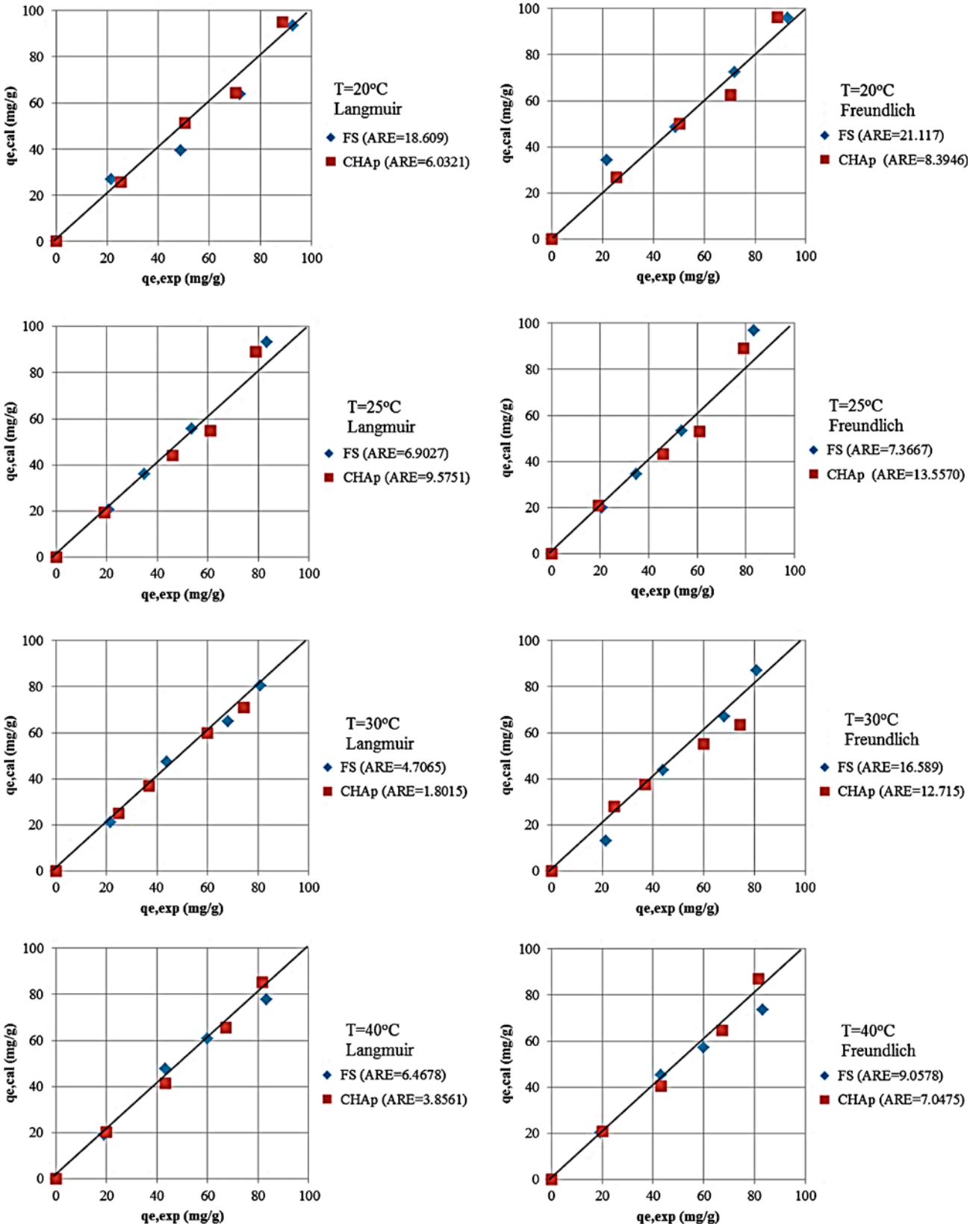

Fig. 12. ARE values and the comparison of Langmuir and Freundlich isotherm models.

Table 7
The kinetic and intraparticle model constants and regression coefficients (initial pH 2.0; temperature: 25°C; adsorbent concentration: 1.0 g/L; contact time: 120 min)

			Pseudo-first-order model constants			Pseudo-second-order model constants			Intraparticle diffusion model constants		
Adsorbent	$C_{o,exp}$ (mg/L)	$q_{e,exp}$ (mg/g)	$q_{e,cal}$	k_1	R^2	$q_{e,cal}$	k_2	R^2	K_i	Intercept	R^2
FS	24	19.2	17.9	0.023	0.856	18.3	0.0088	0.990	1.3	5.4	0.996
	52	48.0	46.8	0.044	0.835	47.7	0.0072	0.998	4.9	17.5	0.993
	78	75.2	74.2	0.053	0.867	75.1	0.0084	0.999	5.1	45.1	0.992
	102	94.4	93.1	0.058	0.799	94.3	0.0062	0.999	5.2	62.9	0.994
CHAp	32	30.4	29.7	0.051	0.921	30.3	0.012	0.996	3.2	7.9	0.999
	50	48.4	45.2	0.048	0.833	47.3	0.0070	0.998	6.9	8.1	0.990
	79	78.4	77.3	0.039	0.697	77.7	0.0074	0.998	11.1	10.9	0.992
	99	98.4	93.1	0.037	0.952	97.2	0.0015	0.991	11.4	23.3	0.994

Notes: $q_{e,cal}$ (mg/g); k_1 (1/min); k_2 (g/mg min); K_i (mg/g $min^{0.5}$).

The evaluation of the diffusion mechanism is not possible with the pseudo-first-order and the PSOKM because the adsorbate molecules are most probably transported from the bulk of the solution into the solid phase through intraparticle diffusion in many adsorption processes. Weber and Morris [55] developed a widely accepted kinetic-based model. It is used to evaluate the intraparticle diffusion and to determine the rate-determining step in adsorption process. The equation representing the Weber–Morris model is as follows:

$$q_t = K_i \cdot t^{0.5} + I \quad (15)$$

If the adsorption process follows the intraparticle diffusion model, a plot of q_t vs. $t^{0.5}$ should be linear and pass through the origin. On the other hand, the slope will be linear but will not pass through the origin when an initial external mass transfer prevails. In this regard, the plot is multilinear for many adsorption systems in the literature like for this study [56,57].

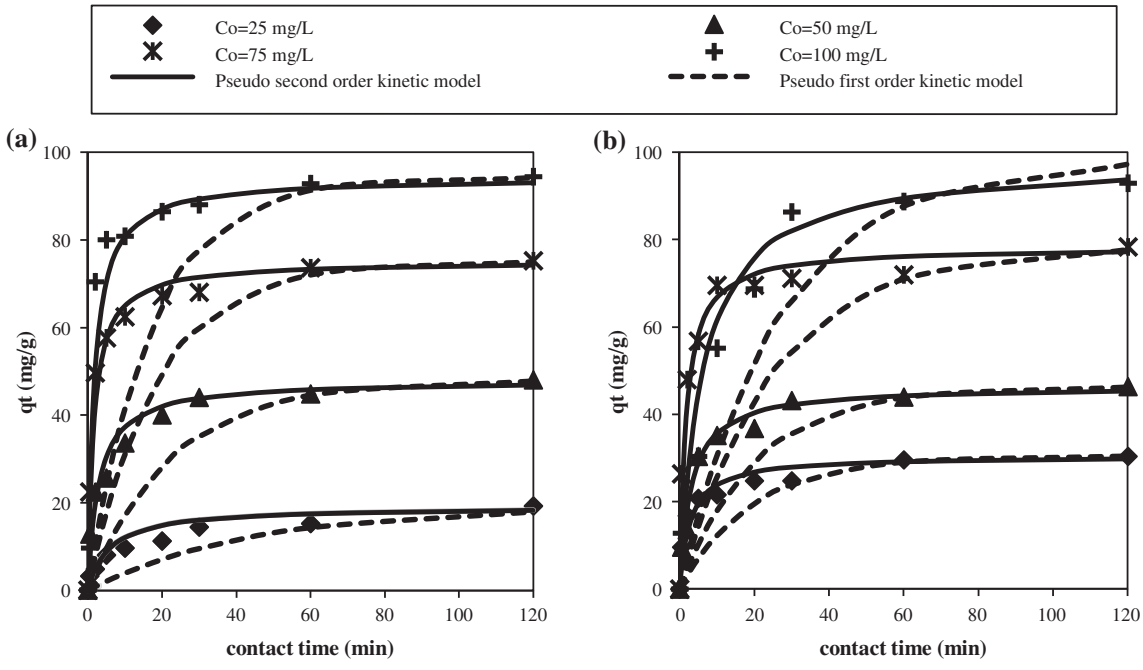

Fig. 13. The comparison of the kinetic models (initial pH 2.0; temperature: 30°C; adsorbent concentration: 1.0 g/L; contact time: 120 min) (a) FS and (b) CHAp.

The effects of intraparticle diffusion on the AB 121 adsorption by FS and CHAp were investigated at different initial dye concentrations and the results were given in Fig. 14(a) and (b) for FS and CHAp, respectively, and Table 7. It was observed from Fig. 14 that there are three linear portions. The initial portion relates to the boundary layer diffusion (film diffusion); the second portion describes the gradual adsorption step, where intraparticle diffusion control is rate limiting; and the last portion represents the adsorption equilibrium, where the intraparticle diffusion starts to decrease due to the exceedingly low concentrations of adsorbate left in the solutions as well as less active adsorption sites. Consequently, the observed multilinearity also suggests that intraparticle diffusion was not only rate-limiting mechanism; both also film diffusion and intraparticle diffusion processes were controlling AB 121 adsorption onto FS and CHAp.

It is necessary to distinguish the rate-limiting step between film diffusion and particle diffusion of adsorbate molecules. Boyd kinetic equation was applied in order to determine the slowest step in the studied adsorption processes. The Boyd model is originally proposed for intraparticle diffusion in ion exchangers and is expressed as [58]:

$$F = 1 - \left(6/\pi^2\right)e^{(-Bt)} \tag{16}$$

where F is the fractional attainment of equilibrium, at different times, t, and Bt is a function of $F = q_t/q_e$.

Eq. (16) can be rearranged by taking the natural logarithm:

$$Bt = -0.4977 - \ln(1 - F) \tag{17}$$

According to Eqs. (16) and (17); if the plot of Bt vs. t is linear and passes through the origin, then the slowest or rate-limiting step in the adsorption process is intraparticle diffusion; if the plot is non-linear or linear but does not pass through the origin, then the adsorption process is controlled by film diffusion.

The plots of Bt vs. t for AB 121 adsorption on FS and CHAp (figure not shown) were employed to distinguish between adsorption controlled by film diffusion and by intraparticle diffusion. The plots were neither linear nor passed through the origin at different initial AB 121 concentrations indicating the film diffusion controlled mechanism.

3.5. Thermodynamic studies

In order to describe the thermodynamic behavior of the adsorption of AB 121 dye anions on FS and CHAp, thermodynamic parameters such as Gibb's free energy change (ΔG), enthalpy change (ΔH) and entropy change (ΔS) were determined using the following equations:

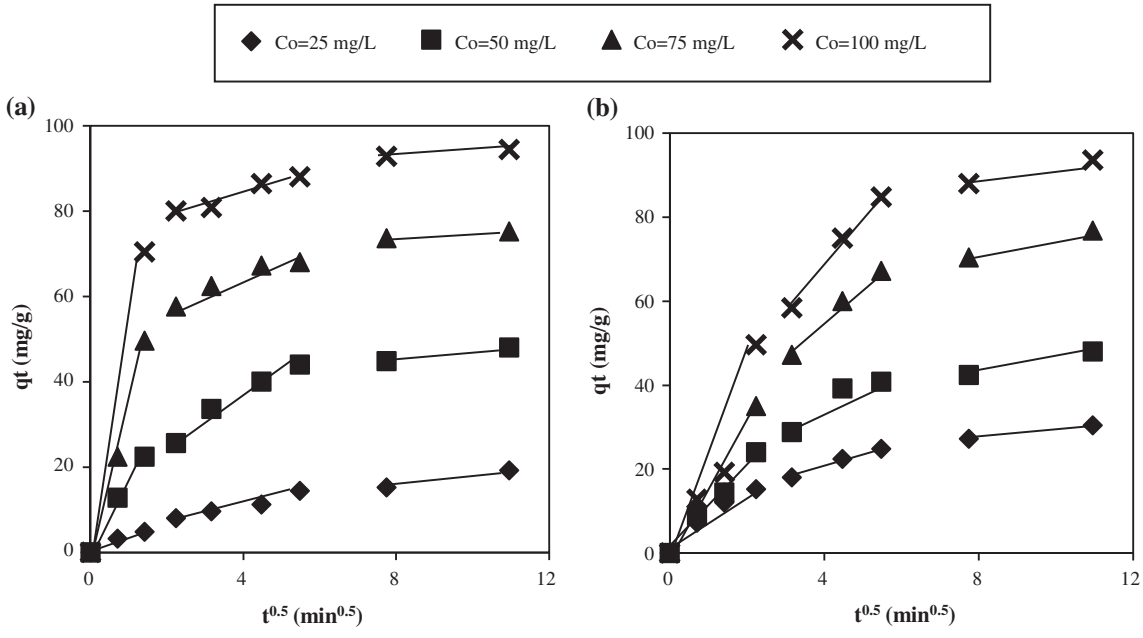

Fig. 14. Plots of intraparticle diffusion model (initial pH 2.0; temperature: 30˚C; adsorbent concentration: 1.0 g/L; contact time: 120 min) (a) FS and (b) CHAp.

$$\Delta G = -RT \ln K_c = \Delta H - T\Delta S \quad (18)$$

$$\ln K_c = [\Delta S/R] - [\Delta H/RT] \quad (19)$$

where R is ideal gas constant (8.314 J/mol.K), T is temperature (K) and K_c ($C_{ad,e}/C_e$) is the equilibrium constant at temperature T. Where $C_{ad,e}$ is the adsorbed dye concentration at equilibrium (mg/L), C_e is the unadsorbed dye concentration at equilibrium (mg/L). If adsorbent concentration is 1.0 g/L, $C_{ad,e}$ is equal to q_e at a given temperature. The Gibb's free energy change values (ΔG) for adsorption of AB 121 on FS and CHAp were calculated from Eq. (18) at different temperatures and were listed in Table 8. According to Eq. (19), the entropy and enthalpy change values can be calculated from the intercept and slope of the plot of ln K_c vs. $1/T$, respectively. The enthalpy (ΔH) and entropy (ΔS) values obtained from the plots ($y = 17{,}932x - 56.2$, $R^2 = 0.988$ for FS; $y = 13{,}281x - 39.7$, $R^2 = 0.999$ for CHAp) were also tabulated in Table 8.

According to Table 8, the values of ΔG were negative at all temperatures and the feasibility of the process and the spontaneous nature of AB 121 adsorption onto FS and CHAp were confirmed with the negative values of ΔG. It was also noted that the ΔG values decreased with increasing temperature. This may also asserted that a better adsorption occurred at lower temperatures due to less available active sites on the surface of adsorbents at higher temperatures. The negative values of ΔH revealed that the adsorption was an exothermic process as expected from the results of temperature optimization studies. The negative ΔS value corresponds to a decrease in randomness at the solid/liquid interface during the sorption of dye on adsorbent while low value of ΔS indicates that no remarkable change on entropy occurs [59]. Chowdhury et al. [48] determined that the malachite green adsorption onto fish (*Labeo rohita*) scales was spontaneous due to the negative values of Gibbs free energies. Also, Vieira et al. [60] evaluated the thermodynamic parameters such as Gibb's free energy (ΔG), entropy (ΔS) and enthalpy (ΔH); and they stated that the adsorption of anionic dyes by fish (*Leporinus elongatus*) scales was spontaneous ($\Delta G < 0$), exothermic ($\Delta H < 0$) and the decreased randomness at the solid/solution interface during the adsorption process ($\Delta S < 0$).

3.6. AB 121 desorption from FS

The regeneration and reuse of the adsorbent are important for the process economy. Regenerations of the dye-loaded adsorbents are evaluated via sequential adsorption–desorption cycles [61]. In this study, before the investigation of the reuse, desorption experiments were carried out to find the optimum desorption pH and desorption yields were calculated. Desorption yields (desorption yield, % = $(C_e/C_o) \times 100$) for 2.0, 4.0, 6.0, 8.0, 10, and 12 values of initial pH at initial AB 121 concentration 100 ± 10 mg/L were found as 2.21, 2.21, 4.42, 13.3, 33.2, and 55.3%, respectively. The results stated that desorption yields positively correlated with initial pH values. The number of negatively charged sites scale up at high pH value, which supported desorption of anionic dye molecules due to electrostatic repulsion. After the optimum initial desorption pH was determined as 12, successive batch adsorption–desorption experiments were conducted for 8.0 cycles. The adsorbed–desorbed yields of each cycle were given in Fig. 15. The data demonstrated that the adsorption capacity decreased as reusing the

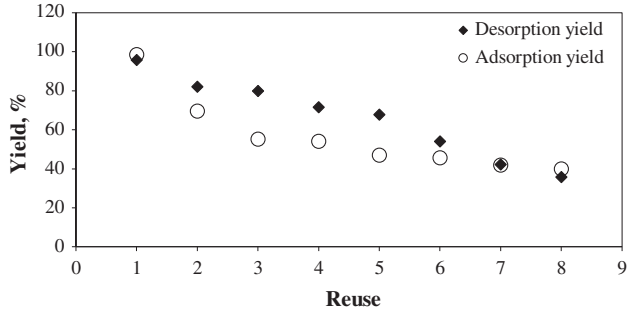

Fig. 15. Adsorption and desorption yields after reuse of FS.

Table 8
Thermodynamic parameters

Adsorbent	Temperature (°C)	ΔG (J/mole)	ΔH (J/mole)	ΔS (J/mole K)
FS	298	−2,438.9	−35,630.9	−111.6
	303	−1,700.7		
	313	−733.0		
CHAp	298	−2,849.4	−26,389.3	−78.9
	303	−2,475.0		
	313	−1,668.5		

adsorbent. While the adsorbed AB 121 amount by FS in the first adsorption cycle was determined as 98.5 mg/g, the adsorbed AB 121 amount at the end of 8.0 adsorption cycle was found as 39.9 mg/g. Consequently, FS displayed high structural stability even after multi-cycles use, hence it is considered that FS can be repeatedly used as an adsorbent to remove the dye anions.

4. Conclusion

In this study, the adsorption of AB 121 on FS, scales of *D. labrax*, CHAp and extracted hydroxyapatite form FS (FHAp) were investigated in a batch system and the results were given as follows:

(1) Optimum initial pH, initial dye concentration, temperature, and adsorbent concentration for AB 121 adsorption on FS and CHAp were determined to be 2.0, 100 mg/L, 30°C, and 1.0 g/L, respectively. The pH_{PZC} values were found as 7.25 for FS and 5.72 for CHAp. At the optimum environmental conditions, the uptake values of FS and CHAp for AB 121 were found as 298.4 and 267.2 mg/g, respectively.
(2) The adsorption equilibrium data of AB 121 by FS and CHAp fitted well to the Langmuir isotherm model. The monolayer coverage capacities calculated from Langmuir isotherm model of FS and CHAp for AB 121 adsorption were found to be 300.7 and 291.5 mg/g, respectively.
(3) It was observed that adsorption kinetics of AB 121 on FS and CHAp can be defined by the PSOKM.
(4) The mechanism of AB 121 adsorption on FS and CHAp is complex and both the surface adsorption as well as intraparticle diffusion contributes to the rate-limiting step. Analysis of adsorption data using Boyd kinetic model confirmed that external mass transfer was the main rate-limiting step in adsorption process.
(5) The thermodynamic parameters such as ΔG, ΔH, and ΔS were determined as negative and showed that the studied adsorption processes were exothermic and spontaneous.
(6) Desorption studies were carried out to evaluate the reusability of FS. The results showed that FS can be repeatedly used as an adsorbent to remove acidic dyes from wastewaters.
(7) The hydroxyapatite extraction from FS was performed using alkaline treatment method and AB 121 adsorption was also studied onto FHAp. At optimum adsorption conditions (initial pH 2.0, initial dye concentration: 100 ± 10 mg/L, temperature: 30°C and adsorbent concentration: 1.0 g/L), the adsorption capacity of FHAp for AB 121 was determined to be 268.8 mg/g.
(8) The characterization of adsorbents was performed with FTIR, XRD, and SEM analysis methods. It was observed that FTIR spectrums, XRD patterns, and SEM images of the studied adsorbents before and after adsorption did not exhibit any differences, which is indicating physical adsorption processes. Moreover, according to FTIR, XRD, and EDX analyses of FS before adsorption, FS contain hydroxyapatite and collagen.
(9) BET analysis results for the studied adsorbents, FS, CHAp, and FHAp, showed that they were porous materials having meso- and macropores with pore volumes of 0.0044, 0.25, and 0.28 cm^3/g, respectively. The specific BET surface areas of FS, CHAp, and FHAp were determined as 0.83, 51.4, and 94.9 m^2/g, respectively.
(10) Consequently, FS and CHAp could be utilized as adsorbent effectively for AB 121 adsorption. Also, hydroxyapatite extracted from FS (FHAp) is a low-cost, effective, environment-friendly, and alternative adsorbent for dye adsorption systems in view of the literature.

Acknowledgments

This work was supported by BAP, Scientific Research Projects Management of Mersin University, Turkey, (BAP-FBE KMB (DU) 2014-1 YL).

Nomenclature

A	—	Temkin constant about binding energy (L/g)
b	—	a constant related to the affinity of the binding sites (L/mg)
B	—	activity coefficient related to adsorption mean free energy ($mole^2\ J^2$)
Bt	—	a function of $F = q_t/q_e$
$C_{ad,e}$	—	adsorbed dye concentration at equilibrium (mg/L)
C_e	—	unadsorbed concentration at equilibrium (mg/L)
CHAp	—	commercial hydroxyapatite
C_o	—	initial dye concentration (mg/L)
$C_{o,exp}$	—	experimental initial dye concentration (mg/L)
$D_{particle}$	—	average particle width (nm)
D_{pore}	—	average pore width (nm)

E — adsorption energy (kJ/mole)
F — fractional attainment of equilibrium
FHAp — hydroxyapatite extracted from *Dicentrarchus labrax* scales
FS — fish (*Dicentrarchus labrax*) scales
K_c — $(C_{ad,e}/C_e)$, the adsorption equilibrium constant at temperature T
K_F — Freundlich constant indicating adsorption capacity $(mg/g)/(L/mg)^{1/n}$)
K_t — Temkin constant about adsorption heat (J/mole)
k_1 — pseudo-first-order kinetic rate constant (1/min)
k_2 — pseudo-second-order kinetic rate constant (g /(mg min))
P — number of measurements
R — ideal gas constant (J/mol K)
S_{BET} — specific BET surface area (m^2/g)
T — temperature (°C, K)
V_{pore} — average pore volume (m^3/g)
q_e — the adsorbed amount per unit mass of adsorbent (mg/g)
$q_{e,cal}$ — the calculated adsorbed amount per unit mass of adsorbent (mg/g)
$q_{e,exp}$ — the experimental adsorbed amount per unit mass of adsorbent (mg/g)
q_m — maximum adsorption capacity (mg/g)
Q^o — maximum monolayer coverage capacity of adsorbent (mg/g)
X_o — adsorbent concentration (g/L)
ε — Polanyi potential (J/mole)
$1/n$ — Freundlich constant indicating adsorption intensity
ΔG — Gibb's free energy change (J/mole)
ΔH — enthalpy change (J/mole)
ΔS — entropy change (J/mole K)

References

[1] V. Karthik, K. Saravanan, K.P. Bharathi, V. Dharanya, C. Meiaraj, An overview of treatments for the removal of textile dyes, JCPS 7(4) (2014) 301–307.
[2] P.V. Nidheesh, R. Gandhimathi, S.T. Ramesh, Degradation of dyes from aqueous solution by Fenton processes: A review, Environ. Sci. Pollut. Res. 20(4) (2013) 2099–2132.
[3] K. Murugesan, I.H. Nam, Y.M. Kim, Y.S. Chang, Decolorization of reactive dyes by a thermostable laccase produced by *Ganoderma lucidum* in solid state culture, Enzyme Microb. Technol. 40 (2007) 1662–1672.
[4] M.M. Ayad, A.A. El-Nasr, Anionic dye (acid green 25) adsorption from water by using polyaniline nanotubes salt/silica composite, J. Nanostruct. Chem. 3 (2012) 1–9.
[5] Y. Anjaneyulu, N. Sreedhara Chary, D. Samuel Suman Raj, Decolourization of industrial effluents—Available methods and emerging technologies—A Review, Rev. Environ. Sci. Biotechnol. 4(4) (2005) 245–273.
[6] J. Carvalho1, A. Ribeiro, J. Graça, J. Araújo, C. Vilarinho, F. Castro, Adsorption process onto an innovative eggshell-derived low-cost adsorbent in simulated effluent and real industrial effluents, in: Wastes: Solutions, Treatments and Opportunities, 1st International Conference, September 12th–14th, 2011.
[7] Q. Zhou, W. Gong, C. Xie, D. Yang, X. Ling, X. Yuan, S. Chen, X. Liu, Removal of Neutral Red from aqueous solution by adsorption on spent cottonseed hull substrate, J. Hazard. Mater. 185 (2011) 502–506.
[8] C.A. Mullen, A.A. Boateng, N.M. Goldberg, I.M. Lima, D.A. Laird, K.B. Hicks, Bio-oil and bio-char production from corn cobs and stover by fast pyrolysis, Biomass Bioenergy 34 (2010) 67–74.
[9] D. Božić, M. Gorgievski, V. Stanković, N. Štrbac, S. Šerbula, N. Petrović, Adsorption of heavy metal ions by beech sawdust—Kinetics, mechanism and equilibrium of the process, Ecol. Eng. 58 (2013) 202–206.
[10] M. Rafatullah, O. Sulaiman, R. Hashim, A. Ahmad, Adsorption of methylene blue on low-cost adsorbents: A review, J. Hazard. Mater. 177 (2010) 70–80.
[11] A. Özer, G. Akkaya, M. Turabik, Biosorption of acid red 274 (AR 274) on *Enteromorpha prolifera* in a batch system, J. Hazard. Mater. B 126 (2005) 119–127.
[12] Y.C. Huang, P.C. Hsiao, H.J. Chai, Hydroxyapatite extracted from fish scale: Effects on MG63 osteoblast-like cells, Ceram. Int. 37 (2011) 1825–1831.
[13] A.C. Dancu, R. Barabas, E.S. Bogya, Adsorption of nicotinic acid on the surface of nanosized hydroxyapatite and structurally modified hydroxyapatite, Cent. Eur. J. Chem. 9 (2011) 660–669.
[14] R. Ansari, Z. Mosayebzadeh, Application of polyaniline as an efficient and novel adsorbent for azo dyes removal from textile wastewaters, Chem. Pap. 65 (2011) 1–8.
[15] V.C. Srivastava, I.D. Mall, I.M. Mishra, Characterization of mesoporous rice husk ash (RHA) and adsorption kinetics of metal ions from aqueous solution onto RHA, J. Hazard. Mater. 134 (2006) 257–267.
[16] S. Kongsri, K. Janpradit, K. Buapa, S. Techawongstien, S. Chanthai, Nanocrystalline hydroxyapatite from fish scale waste: Preparation, characterization and application for selenium adsorption in aqueous solution, Chem. Eng. J. 215–216 (2013) 522–532.
[17] G.Z. Kyzas, N.K. Lazaridis, A.C. Mitropoulos, Removal of dyes from aqueous solutions with untreated coffee residues as potential low-cost adsorbents: Equilibrium, reuse and thermodynamic approach, Chem. Eng. J. 189–190 (2012) 148–159.
[18] F.G. Torres, O.P. Troncoso, J. Nakamatsu, C.J. Grande, C.M. Gómez, Characterization of the nanocomposite laminate structure occurring in fish scales from *Arapaima Gigas*, Mater. Sci. Eng. C 28(8) (2008) 1276–1283.
[19] A. Ślósarczyk, Z. Paszkiewicz, C. Paluszkiewicz, FTIR and XRD evaluation of carbonated hydroxyapatite powders synthesized by wet methods, J. Mol. Struct. 744–747 (2005) 657–661.
[20] R. Ravarian, F. Moztarzadeh, M.S. Hashjin, S.M. Rabiee, P. Khoshakhlagh, M. Tahriri, Synthesis, characterization and bioactivity investigation of bioglass/hydroxyapatite composite, Ceram. Int. 36 (2010) 291–297.
[21] L.N. Du, B. Wang, G. Li, S. Wang, D.E. Crowley, Y.H. Zhao, Biosorption of the metal-complex dye Acid

Black 172 by live and heat-treated biomass of *Pseudomonas* sp. strain DY1: Kinetics and sorption mechanisms, J. Hazard. Mater. 205–206 (2012) 47–54.
[22] S. Mondal, R. Bardhan, B. Mondal, A. Dey, S.S. Mukhopadhyay, S. Roy, R. Guha, K. Roy, Synthesis, characterization and in vitro cytotoxicity assessment of hydroxyapatite from different bioresources for tissue engineering application, Bull. Mater. Sci. 35 (2012) 683–691.
[23] S.V. Mohan, S.K. Mohan, J. Karthikeyan, IR, XRD and SEM studies to elucidate the mechanism of azo dye sorption interaction with coal based adsorbents and activated carbon from aqueous phase, J. Sci. Ind. Res. 60(5) (2001) 410–415.
[24] M. Sato, M.A. Sambito, A. Aslani, N.M. Kalkhoran, E.B. Slamovich, T.J. Webster, Increased osteoblast functions on undoped and yttrium-doped nanocrystalline hydroxyapatite coatings on titanium, Biomaterials 27(11) (2006) 2358–2369.
[25] R. Joseph, W.J. McGregor, M.T. Martyn, K.E. Tanner, P.D. Coates, Effect of hydroxyapatite morphology/surface area on the rheology and processability of hydroxyapatite filled polyethylene composites, Biomaterials 2321 (2002) 4295–4302.
[26] A. Banerjee, A. Bandyopadhyay, S. Bose, Hydroxyapatite nanopowders: Synthesis, densification and cell–materials interaction, Mater. Sci. Eng., C 27(4) (2007) 729–735.
[27] A. Venugopal, M.S. Scurrell, Hydroxyapatite as a novel support for gold and ruthenium catalysts: Behaviour in the water gas shift reaction, Appl. Catal., A 245(1) (2003) 137–147.
[28] K.C.B. Yeong, J. Wang, S.C. Ng, Mechanochemical synthesis of nanocrystalline hydroxyapatite from CaO and $CaHPO_4$, Biomaterials 22(20) (2001) 2705–2712.
[29] V.K. Gupta, B. Gupta, A. Rastogi, S. Agarwal, A. Nayak, A comparative investigation on adsorption performances of mesoporous activated carbon prepared from waste rubber tire and activated carbon for a hazardous azo dye—Acid Blue 113, J. Hazard. Mater. 186(1) (2011) 891–901.
[30] K.Y. Foo, B.H. Hameed, Factors affecting the carbon yield and adsorption capability of the mangosteen peel activated carbon prepared by microwave assisted K_2CO_3 activation, Chem. Eng. J. 180 (2012) 66–74.
[31] S. Banerjee, M.C. Chattopadhyaya, Adsorption characteristics for the removal of a toxic dye, tartrazine from aqueous solutions by a low cost agricultural by-product, Arab. J. Chem. (in press), doi: 10.1016/j.arabjc.2013.06.005.
[32] L.S.A.A. Al-Amri, M.H.H.A. Subhi, R. Namdeti, Comparison Studies for the removal of methylene blue from aqueous solution using tea and coffee powder, Int. J. ChemTech Res. 6 (2014) 619–627.
[33] H. Izanloo, S. Nasseri, Cadmium removal from aqueous solutions by ground pine cone, Iran J. Environ. Health 2 (2005) 33–42.
[34] A. Özer, D. Özer, A. Özer, The adsorption of copper (II) ions on to dehydrated wheat bran (DWB): Determination of the equilibrium and thermodynamic parameters, Process Biochem. 39(12) (2004) 2183–2191.
[35] R.E. Treybal, Mass Transfer Operations, third ed., McGraw-Hill Book Company, Singapore, 1981.
[36] Z. Aksu, Aİ. Tatlı, Ö. Tunç, A comparative adsorption/biosorption study of Acid Blue 161: Effect of temperature on equilibrium and kinetic parameters, Chem. Eng. J. 142 (2008) 23–39.
[37] I. Langmuir, The adsorption of gases on plane surfaces of glass, mica and platinum, J. Am. Chem. Soc. 40 (1918) 1361–1403.
[38] H.M.F. Freundlich, Über die adsorption in lösungen, (About the adsorption in solutions) Z. Phys. Chem. 57 (1906) 385–470.
[39] M.J. Temkin, V. Pyzhev, Recent modifications to Langmuir isotherms, Acta Physiochim. USSR 12 (1940) 217–222.
[40] M.M. Dubinin, L.V. Radushkevich, Equation of the characteristics curve of activated charcoal, Chem. Zent. 1 (1947) 875.
[41] E. Daneshvar, M. Kousha, M. Jokar, N. Koutahzadeh, E. Guibal, Acidic dye biosorption onto marine brown macroalgae: Isotherms, kinetic and thermodynamic studies, Chem. Eng. J. 204–206 (2012) 225–234.
[42] N. Barka, S. Qourzal, A. Assabbane, A. Nounah, Y. Aît-Ichou, Adsorption of Disperse Blue SBL dye by synthesized poorly crystalline hydroxyapatite, J. Environ. Sci. 20(10) (2008) 1268–1272.
[43] R. Nadeem, T.M. Ansari, A.M. Khalid, Fourier transform infrared spectroscopic characterization and optimization of Pb(II) biosorption by fish (*Labeo rohita*) scales, J. Hazard. Mater. 156(1–3) (2008) 64–73.
[44] A. Basu, S. Mustafiz, M.R. Islam, N. Bjorndalen, M.S. Rahaman, O. Chaalal, A comprehensive approach for modeling sorption of lead and cobalt ions through fish scales as an adsorbent, Chem. Eng. Commun. 193(5) (2006) 580–605.
[45] J.F. Villanueva-Espinosa, M. Hernández-Esparza, F.A. Ruiz-Treviño, Adsorptive properties of fish scales of *Oreochromis niloticus* (Mojarra Tilapia) for metallic ion removal from waste water, Ind. Eng. Chem. Res. 40 (16) (2001) 3563–3569.
[46] N. Barka, S. Qourzal, A. Assabbane, A. Nounah, Y. Ait-Ichou, Removal of Reactive Yellow 84 from aqueous solutions by adsorption onto hydroxyapatite, J. Saudi Chem. Soc. 15(3) (2011) 263–267.
[47] K.O. Moura, E.F.S. Vieira, A.R. Cestari, Poly(glutaraldehyde)-stabilized fish scale fibrillar collagen-some features of a new material for heavy metal sorption, J. Appl. Polym. Sci. 124(4) (2012) 3208–3221.
[48] S. Chowdhury, P. Das Saha, U. Ghosh, Fish (*Labeo rohita*) scales as potential low-cost biosorbent for removal of malachite green from aqueous solutions, Biorem. J. 16 (2012) 235–242.
[49] K.O. Moura, E.F.S. Vieira, A.R. Cestari, The use of solution microcalorimetry to evaluate chemically modified fish scales as a viable adsorbent for heavy metals, J. Therm. Anal. Calorim. 107(3) (2012) 999–1005.
[50] K. Lin, J. Pan, Y. Chen, R. Cheng, X. Xu, Study the adsorption of phenol from aqueous solution on hydroxyapatite nanopowders, J. Hazard. Mater. 161(1) (2009) 231–240.
[51] S. Kongsri, K. Janpradit, K. Buapa, S. Techawongstien, S. Chanthai, Nanocrystalline hydroxyapatite from fish scale waste: Preparation, characterization and application for selenium adsorption in aqueous solution, Chem. Eng. J. 215–216 (2013) 522–532.

[52] D. Vu, Z. Li, H. Zhang, W. Wang, Z. Wang, X. Xu, B. Dong, C. Wang, Adsorption of Cu(II) from aqueous solution by anatase mesoporous TiO_2 nanofibers prepared via electrospinning, J. Colloid Interface Sci. 367 (1) (2012) 429–435.
[53] A. Özer, M. Turabik, Competitive biosorption of acid dyes from binary solutions onto *Enteromorpha prolifera*: Application of the first order derivative spectrophotometric analysis method, Sep. Sci. Technol. 45(3) (2010) 380–393.
[54] Y.S. Ho, G. Mckay, Kinetic models for the sorption of dye from aqueous solution by wood, Process Saf. Environ. 76 (1998) 183–191.
[55] W.J. Weber Jr., J.C. Morris, Kinetics of adsorption on carbon from solution, J. Sanit. Eng. Div. Am. Soc. Civ. Eng. 89 (1963) 31–59.
[56] M. Toor, B. Jin, Adsorption characteristics, isotherm, kinetics, and diffusion of modified natural bentonite for removing diazo dye, Chem. Eng. J. 187 (2012) 79–88.
[57] M. Islam, P.C. Mishra, R. Patel, Arsenate removal from aqueous solution by cellulose-carbonated hydroxyapatite nanocomposites, J. Hazard. Mater. 189 (3) (2011) 755–763.
[58] T. Maiyalagan, S. Karthikeyan, Film-pore diffusion modeling for sorption of azo dye on to exfoliated graphitic nanoplatelets, Indian J. Chem. Technol. 20 (2013) 7–14.
[59] J. Kluczka, T. Korolewicz, M. Zołotajkin, W. Simka, M. Raczek, A new adsorbent for boron removal from aqueous solutions, Environ. Technol. 34 (2013) 1369–1376.
[60] E.F. Vieira, A.R. Cestari, W.A. Carvalho, C. dos S. Oliveira, R.A. Chagas, The use of freshwater fish scale of the species *Leporinus elongatus* as adsorbent for anionic dyes, J. Therm. Anal. Calorim. 109(3) (2012) 1407–1412.
[61] G.Z. Kyzas, N.K. Lazaridis, D.N. Bikiaris, Optimization of chitosan and β-cyclodextrin molecularly imprinted polymer synthesis for dye adsorption, Carbohydr. Polym. 91 (2013) 198–208.